


# Accurate Optical Number Density Measurement of $^{12}\text{CO}_2$ and $^{13}\text{CO}_2$ with Direct Frequency Comb Spectroscopy

Sarah K. Scholten,<sup>\*</sup> Christopher Perrella, James D. Anstie, Richard T. White, and Andre N. Luiten  
*Institute for Photonics and Advanced Sensing, School of Physical Sciences, The University of Adelaide, Adelaide,  
 South Australia 5005, Australia*

 (Received 14 January 2019; revised manuscript received 10 June 2019; published 23 September 2019)

We report on the use of direct frequency comb spectroscopy to accurately measure the concentrations of  $^{12}\text{C}^{16}\text{O}_2$  and  $^{13}\text{C}^{16}\text{O}_2$  isotopologs in a gas sample. We demonstrate an accuracy of 0.5% and 12% for concentration measurements of  $^{12}\text{C}^{16}\text{O}_2$  and  $^{13}\text{C}^{16}\text{O}_2$ , respectively, with the measured isotopic ratio in excellent agreement with that expected from their natural abundances. The precision of the concentration measurements is also high, at 0.03% and 1.24% for  $^{12}\text{C}^{16}\text{O}_2$  and  $^{13}\text{C}^{16}\text{O}_2$ , respectively. The measurement technique is verified to be highly linear for concentrations ranging over 3 orders of magnitude. Direct frequency comb spectroscopy can be applied to numerous molecular species, and is therefore a promising technique for measurements in environmental monitoring and biomedical sciences.

DOI: [10.1103/PhysRevApplied.12.034045](https://doi.org/10.1103/PhysRevApplied.12.034045)

## I. INTRODUCTION

Accurate measurement of the isotopic composition of a gas sample is useful in a wide variety of applications. The  $^{13}\text{C}^{12}\text{C}$  ratio of  $\text{CO}_2$  is particularly important in the environmental sciences, including paleoclimatology [1,2], carbon cycling studies [3–5], oceanography [6], atmospheric science [7], and monitoring of greenhouse-gas emissions, sequestration, and storage integrity [8,9]. Isotopic analysis is also used in biomedical applications, including metabolic flux analysis [10,11], detection of the bacterium *Helicobacter pylori* (which causes gastric ulcers and gastric cancers) [11], and assessment of liver function and disease, gastric emptying, bacterial overgrowth, and pancreatic function [11].

To correctly measure the relative concentrations of isotopologs, techniques with high precision, high accuracy, a large dynamic range, and of course isotopolog differentiability are required. A commonly used technique is mass spectrometry, which fulfills most of these requirements but typically suffers from an inability to differentiate between species of similar atomic mass (e.g.,  $^{13}\text{C}^{16}\text{O}_2$  and  $^{16}\text{O}^{12}\text{C}^{17}\text{O}$ ). More recently, instruments based on optical spectroscopy have been developed to measure isotopic ratios by exploitation of the nuclear-mass-dependent frequency shifts of the ro-vibrational absorption peaks [12].

These optical techniques include cavity ring-down spectroscopy [11–13], Fourier-transform infrared (FTIR) spectroscopy [14,15], dual-comb spectroscopy [16], and direct

frequency comb spectroscopy (DFCS) [17,18]. While possessing excellent precision and accuracy, cavity ring-down spectroscopy requires many sequential measurements as the interrogation laser frequency is scanned, and makes complex gas analysis cumbersome when it is necessary to have a large scan range. FTIR spectroscopy overcomes this by measuring many chemical absorption signatures at once; however, this comes at the expense of long data-acquisition times. Without careful calibration, FTIR spectroscopy can result in inaccurate wavelength determination due to imperfections in the mechanical scans. Dual-comb spectroscopy has been used to measure  $\text{CO}_2$  molecular spectra for  $^{13}\text{C}$  and  $^{12}\text{C}$  in open-air paths; however, this technique requires two optical frequency combs, making the system relatively costly and complex. Nonetheless, recent work on miniaturizing frequency combs might eventually offer a rational way forward in this area [19–23].

In the work reported in this paper we use direct frequency comb spectroscopy without an enhancement cavity to analyze the  $^{12}\text{C}^{16}\text{O}_2$  and  $^{13}\text{C}^{16}\text{O}_2$  isotopologs of  $\text{CO}_2$ . We demonstrate accurate, highly precise, and linear extraction of the concentration of both isotopologs over a large dynamic range. DFCS has been used for isotopic analysis of  $\text{CO}_2$  before but only with an enhancement cavity [17]. The spectroscopy method used in this work operates in the eye-safe near-infrared spectral band, and has the additional benefits of requiring only a single frequency comb as a light source, which is measured with a fixed and robust spectrometer based on spatial frequency dispersion. This reduction in complexity makes the system appealing for applications outside the laboratory.

<sup>\*</sup>sarah.scholten@adelaide.edu.au

## II. EXPERIMENTAL METHODS

### A. Optical experiment

The experimental setup is shown in Fig. 1. An optical frequency comb (Menlo Systems FC1500) is used as the interrogation source, which spans approximately 1500–1600 nm. The carrier-envelope-offset frequency ( $f_{\text{CEO}}$ ) of the comb is locked to a cesium-beam clock (Datum CsIII), while the repetition rate,  $f_{\text{rep}} \approx 250$  MHz, is stabilized by our locking one comb mode to a cavity-stabilized reference laser (NKT Koheras Boostik E15) at 1560 nm. The comb light is split into two paths by a 50:50 fiber coupler. The first path is used for spectroscopy and is further split into two paths, with use of a wedged beam splitter, into the reference path (for optical comparison) and the sample path, which contains a double-passed 3.25-m-long sample cell ( $296 \pm 1$  K) at atmospheric pressure. A gas mixer (EnviroNics Series 2000) uses  $\text{N}_2$  as a buffer gas to adjust the  $\text{CO}_2$  concentration within the sample cell, with the  $\text{CO}_2$  gas containing a natural abundance of  $\text{CO}_2$  isotopologs. The second fiber-coupler output is sent to a length-stabilized low-finesse (approximately 200) Fabry-Perot cavity with bandwidth of approximately 50 MHz that transmits every 36th comb mode. The filtered optical frequency comb is sufficiently sparse that the spectrometer can isolate each mode, which allows identification and assignment of a relative frequency to each comb mode, allowing calibration of the relative frequency axis (to within an overall frequency offset) [24–26].

Automated shutters select light from the sample, reference, and cavity paths, with the collinearity of all three paths ensured by coupling via a four-port 50:50 coupler. The spectrometer is based on a virtually-imaged-phased-array (VIPA) etalon (Light Machinery) with a finesse of approximately 100 and free spectral range of approximately 50 GHz, which spreads the comb light vertically as a function of wavelength [27]. The VIPA is followed by a diffraction grating with 600 lines/mm to remove frequency ambiguity of the VIPA by dispersing the beam

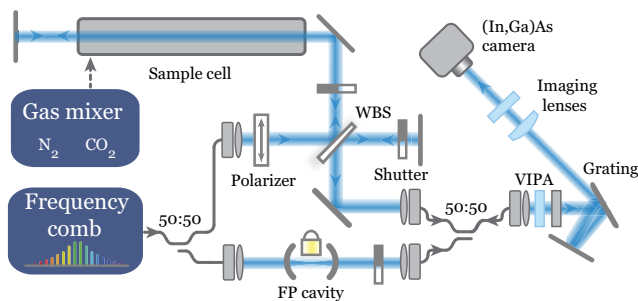


FIG. 1. A simplified diagram of the experiment. Fiber-coupled paths are shown in gray, and free-space optical paths are shown in blue for the optical frequency comb. FP, Fabry-Perot; WBS, wedged beam splitter.

horizontally [28]. This results in a two-dimensional array of comb modes imaged on an (In,Ga)As IR camera (Xenics XEVA-1.7-320), with a spectral range of approximately 2.9 THz (approximately 25 nm) in the horizontal direction and just over one VIPA free spectral range in the vertical direction. Two images are acquired for both the reference path and the sample path; one bright image, followed by a dark image with matched integration time for camera-dark-field subtraction.

### B. Image analysis

To extract the  $\text{CO}_2$  absorption signature from the images taken by the spectrometer [26], the dark frames are first subtracted from each bright image before a pixel-by-pixel camera nonlinearity correction is applied. To reduce noise, 100 measurements of each of the sample and reference images are averaged together. To ascertain the accuracy and precision of the measurements, ten nominally identical sets of 100 images are taken for statistical purposes. The procedure to extract the absorption signature from these averaged images may be found in more detail in Refs. [25,26]. As described in Ref. [26], we use the optically filtered comb image (with an effective mode spacing of 9 GHz), together with the known repetition rate and offset frequency of the comb, to derive an accurate mapping from the position on the detector to the relative optical frequency.

### C. Spectral fitting and number density extraction

A concentration measurement of  $^{12}\text{C}^{16}\text{O}_2$  and  $^{13}\text{C}^{16}\text{O}_2$ , and hence the isotopic ratio, is obtained by our fitting the experimental spectrum with a model absorption spectrum based on parameters from the HITRAN 2012 database [29,30]. There are differences in the optical transfer function of the signal and reference paths due to effects such as beam divergence, etalons, and polarization rotation between paths. This broad-scale background is measured by our filling the sample cell with  $\text{N}_2$  to remove any absorption features and then fitted with an eighth-order Fourier series containing eight cosine and eight sine components. This model is then used to remove the broad-scale background variations from each spectrum recorded as a result of this difference in optical transfer function between paths. Any slight shot-to-shot variations from this background, originating from alignment fluctuations, are accounted for with an additional third-order polynomial. There are three absorption bands that fall within the observed spectral region: the  $30012 \leftarrow 00001$  overtone band of  $^{13}\text{C}^{16}\text{O}_2$  and the  $30013 \leftarrow 00001$  and  $31113 \leftarrow 01101$  overtone and hot band, respectively, of  $^{12}\text{C}^{16}\text{O}_2$ , totaling 307 ro-vibrational features, which are all modeled as Voigt line shapes. The parameters of each peak are available from the HITRAN database, including line strengths [ $S_{\eta\eta'}(T_{\text{ref}})$ ], where  $\eta$  and  $\eta'$  denote the lower

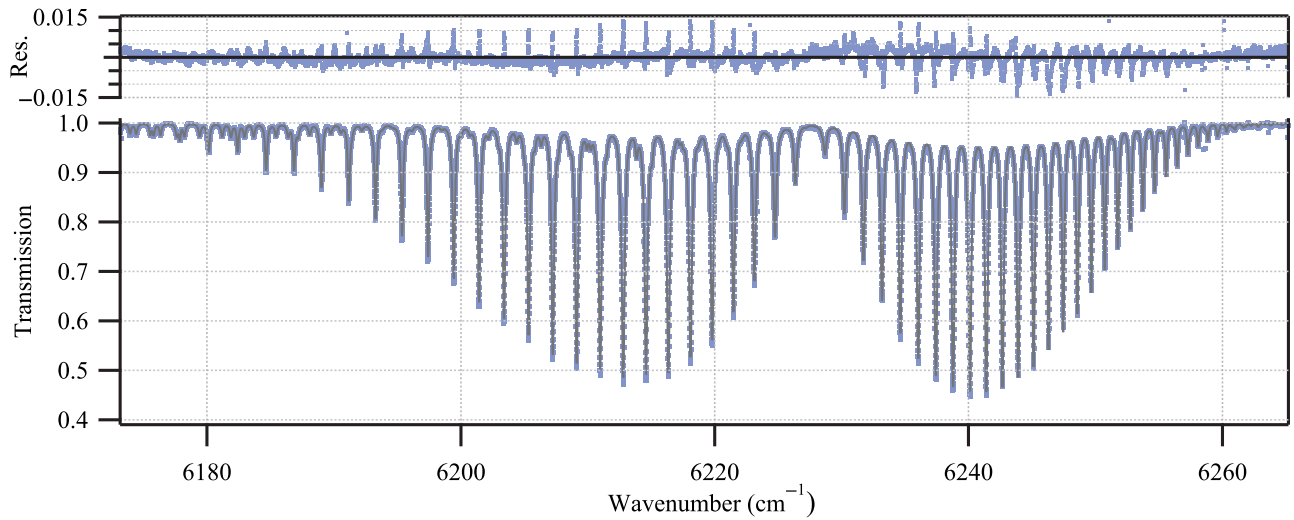


FIG. 2. Data for a pure CO<sub>2</sub> gas sample averaged 1000 times (blue markers) showing the <sup>13</sup>C<sup>16</sup>O<sub>2</sub> 30012 ← 00001 spectral band and the <sup>12</sup>C<sup>16</sup>O<sub>2</sub> 30013 ← 00001 and 31113 ← 01101 overtone and hot band, respectively. A fit (gray) to the 307 ro-vibrational features is shown. Fit residuals (top) show peak-height issues due to the use of the HITRAN-recommended Voigt line profile and some broad-scale structure as the spectrum and background are not separable during fitting.

and upper states of the transition, respectively, line centers ( $\nu_{\eta\eta'}$ ), the lower state energy of the transition ( $E_{\eta}$ ), pressure shifts, and pressure-broadened line half widths due to both air and self-broadening. The spectrometer imposes an instrumental broadening on the spectrum, the shape of which is close to that of a Voigt function with a Lorentzian half width at half maximum of  $0.01 \pm 0.001 \text{ cm}^{-1}$  and Gaussian  $1/e$  half width of  $0.012 \pm 0.001 \text{ cm}^{-1}$ . We obtain this through observation of individual comb modes using the optically filtered frequency comb image. Doppler broadening of  $0.06841 \pm 0.00002 \text{ cm}^{-1}$  for each absorption line is also included in the model. The HITRAN parameters are provided at a reference temperature  $T_{\text{ref}}$  of 296 K. This requires a temperature correction to be included for certain parameters, including the line strength:

$$S_{\eta\eta'}(T) = S_{\eta\eta'}(T_{\text{ref}}) \frac{Q(T_{\text{ref}})}{Q(T)} \frac{e^{-\frac{c_2 E_{\eta}}{T}}}{e^{-\frac{c_2 E_{\eta}}{T_{\text{ref}}}}} \frac{1 - e^{-\frac{c_2 \nu_{\eta\eta'}}{T}}}{1 - e^{-\frac{c_2 \nu_{\eta\eta'}}{T_{\text{ref}}}}}, \quad (1)$$

where  $c_2 = hc/k_B$ ,  $h$  is the Planck constant,  $c$  is the speed of light in a vacuum, and  $k_B$  is the Boltzmann constant [30]. The total internal partition function [ $Q(T)$ ] of each isotopolog must also be altered for temperature, with the full calculation simplified by use of a polynomial approximation [31].

We perform a least-squares optimized fitting of the model to the experimental spectrum, with the only free parameters being the two isotopolog number densities, the temperature, and background terms. The fitted and experimental spectrum for a pure sample of CO<sub>2</sub> is shown in

Fig. 2 for 1000 averages, with an enlarged portion shown in Fig. 3. Underestimation of the peak heights is apparent as seen in the blue residuals and is a known problem with the use of the Voigt line shape recommended for use with the HITRAN database by the HITRAN collaboration,

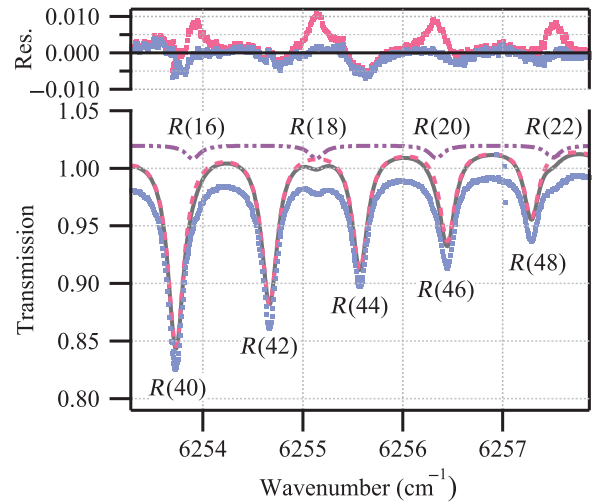


FIG. 3. Enlargement of of the R16–R22 features of the 30012 ← 00001 spectral band of <sup>13</sup>C<sup>16</sup>O<sub>2</sub> among the much-larger R40–R46 lines of the 30013 ← 00001 band of <sup>12</sup>C<sup>16</sup>O<sub>2</sub>. Note the odd-numbered transitions are forbidden due to molecular symmetry [32]. The main graph shows the total fit as a solid gray line, data in blue markers, the <sup>13</sup>C<sup>16</sup>O<sub>2</sub> fit as a dot-dashed purple line, and the <sup>12</sup>C<sup>16</sup>O<sub>2</sub> fit as a dashed pink line. Fits are offset by +0.02. In the residuals graph, blue dots are residuals of data from the total fit and pink dots are residuals of data from the total fit with the <sup>13</sup>C<sup>16</sup>O<sub>2</sub> contributions omitted.

which does not take into account more-complex collisional dynamics [33–37].

### III. RESULTS

To demonstrate the spectrometer’s ability to accurately measure the ratio of isotopologs over a wide range of absorption strengths (or concentrations), we present the spectrometer with gas mixtures made up of  $\text{CO}_2$  and  $\text{N}_2$ . Measurements are made at  $\text{CO}_2:\text{N}_2$  concentration ratios in the sample cell of 100%, 75%, 50%, 25%, and 10%. The analysis is applied to extract the number density of the two targeted isotopologs for the five  $\text{CO}_2$  concentrations examined. Figure 4 shows the measured number density of both isotopologs against those predicted by a third-order-corrected ideal-gas-law calculation (dashed gray line) [38,39]. Isotopic ratio measurements are shown in Fig. 5, and are in excellent agreement with the natural-abundance values of 98.420% and 1.106% for  $^{12}\text{C}^{16}\text{O}_2$  and  $^{13}\text{C}^{16}\text{O}_2$ , respectively, with the remaining isotopologs present in trace amounts [38]. The measurements have a precision of 0.03% and 1.24% for the 100%  $\text{CO}_2$  measurement for  $^{12}\text{C}^{16}\text{O}_2$  and  $^{13}\text{C}^{16}\text{O}_2$ , respectively. The measurement precision is taken to be the standard deviation of ten concentration measurements, each of which is retrieved from fits to a spectrum containing 100 spectra averaged together.

The accuracy of the  $^{12}\text{C}^{16}\text{O}_2$  density measurements is in agreement with the virial-corrected ideal-gas law to within 0.5%, while the  $^{13}\text{C}^{16}\text{O}_2$  measurements agree to within 12%. The discrepancy for  $^{13}\text{C}^{16}\text{O}_2$  arises from the small absorption (only approximately 1%) when compared

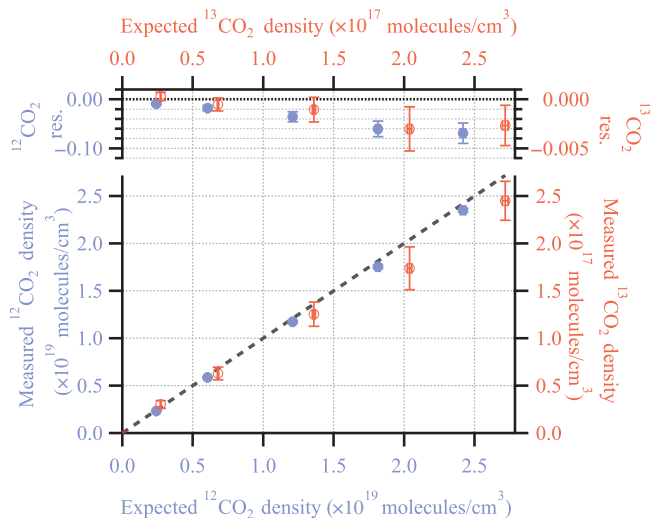


FIG. 4. Average measured densities of  $^{13}\text{C}^{16}\text{O}_2$  (open red circles) and  $^{12}\text{C}^{16}\text{O}_2$  (filled blue circles) for ten sets (reference and signal) of 100 images against densities predicted by the virial-corrected ideal-gas law. The expected 1:1 density line is shown in dashed gray [38].

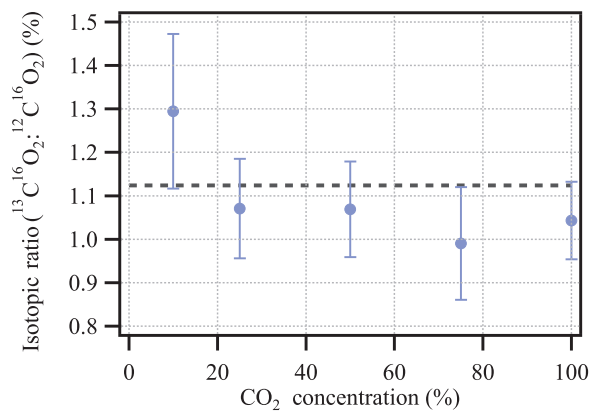


FIG. 5. The measured  $^{13}\text{C}^{16}\text{O}_2:^{12}\text{C}^{16}\text{O}_2$  isotopic ratio derived from ten sets (reference and signal) of 100 images for each  $\text{CO}_2$  concentration against gas-mixer concentration (blue markers). Error bars are a quadrature sum (see the main text). The ratio predicted by the HITRAN database is shown in dashed gray for the natural abundances of the isotopologs in question.

with the  $^{12}\text{C}^{16}\text{O}_2$  peaks, as seen in Fig. 3. The accuracy of our optical concentration measurements, shown in Fig. 4, is limited by four major contributors: the residual background transmission structure, uncertainties in the known absorption strengths and shape of the spectral lines, and spectral broadening from the VIPA. Residual background structure was unable to be adequately fitted as the background and absorption spectra are not completely separable. This contributes uncertainties of 0.2% and 8% to the measured concentrations of  $^{12}\text{C}^{16}\text{O}_2$  and  $^{13}\text{C}^{16}\text{O}_2$ , respectively. The uncertainties in the absorption-line strengths are taken from HITRAN [37]. Assuming the errors for each peak are uncorrelated, we estimate the weighted standard error in the ensemble of  $S_{\eta\eta'}$  to be 0.1% for  $^{12}\text{C}^{16}\text{O}_2$  and 0.3% for  $^{13}\text{C}^{16}\text{O}_2$  [40,41]. These values are calculated by our weighting the quoted error for each line by the absorption-line strength and summing over the ensemble for each isotopolog. Correspondingly, smaller absorption features result in a higher error for  $^{13}\text{C}^{16}\text{O}_2$ . These uncertainties set the ultimate accuracy limit of the spectrometer, and form the limit for all optical spectroscopy isotopolog-concentration measurements. Increases in the accuracy of HITRAN line strengths would in turn increase the accuracy of the spectral fitting and extracted number densities. Another contributor to the error is the use of the HITRAN-recommended Voigt molecular line shape, which has been shown to lead to underestimates of line intensities in high-resolution spectral measurements [33,37]. The slight asymmetry and frequency dependence in the VIPA spectrometer broadening is not accounted for during fitting, with the net effect of each on the density estimated at 0.4% for both isotopologs [26]. This issue can be removed by use of the rarefied comb to interrogate the gas, which completely eliminates

TABLE I. Optical uncertainties and their relative effect on number density measurements.

Effect	$^{12}\text{CO}_2$ (%)	$^{13}\text{CO}_2$ (%)
HITRAN 2012 $S_{\eta\eta'}$ ( $T_{\text{ref}}$ ) uncertainty	0.1	0.3
Spectrometer broadening and asymmetry	0.4	0.4
Residual background structure	0.2	8.0
Combined optical uncertainty	0.5	8.0

The uncertainties listed are percentages of the measured number density at the  $1\sigma$  level for  $^{12}\text{CO}_2$  and  $^{13}\text{CO}_2$ . Detailed discussion of the derivation of the values can be found in the main text.

spectrometer broadening [24]. These optical uncertainties, listed in Table I, are combined in quadrature with the measurement precision to yield total uncertainties of 0.5% and 12% for the  $^{12}\text{C}^{16}\text{O}_2$  and  $^{13}\text{C}^{16}\text{O}_2$  absolute number density measurements, respectively, which are displayed as the error bars in Figs. 4 and 5. The gas mixer has a specified accuracy of 0.75% of the requested concentration for both  $\text{N}_2$  and  $\text{CO}_2$ ; this is displayed as the horizontal error bars in Fig. 4 for both isotopologs.

Agreement of the measured isotopic ratio with the natural-abundance value (Fig. 5) over the full range of  $\text{CO}_2$  concentrations examined demonstrates the excellent linearity of the concentration measurements by the DFCS technique. Deviations from a linear measurement,  $\Delta L$ , are quantified by our taking the ratio of two concentrations  $u_1$  and  $u_2$ , scaled by their known  $\text{CO}_2:\text{N}_2$  ratios,  $r_1$  and  $r_2$ :

$$\Delta L = 1 - \frac{u_1}{r_1} \bigg/ \frac{u_2}{r_2}. \quad (2)$$

If the measurement is linear, each ratio  $u_1/r_1$  and  $u_2/r_2$  should produce the same measured concentration. Our taking all possible comparisons such that  $r_1 > r_2$  and  $u_1 > u_2$  gave a deviation from a linear measurement of  $(-0.15 \pm 0.47)\%$  for  $^{12}\text{C}^{16}\text{O}_2$  measurements. The  $^{13}\text{C}^{16}\text{O}_2$  concentration measurements gave a deviation from linearity of  $(-2.6 \pm 8.6)\%$ , with increased error due to a lower signal-to-noise ratio. Comparison between  $^{12}\text{C}^{16}\text{O}_2$  and  $^{13}\text{C}^{16}\text{O}_2$  over a concentration range of 3 orders of magnitude gave a deviation of linearity of  $(-4.9 \pm 8.5)\%$ , again limited by the signal-to-noise ratio of the  $^{13}\text{C}^{16}\text{O}_2$  absorption peaks. This demonstrates a large dynamic range of highly linear concentration measurements, which can be increased with more averaging and/or a longer absorption path length.

#### IV. CONCLUSION

We demonstrate accurate concentration retrieval of the  $^{12}\text{C}^{16}\text{O}_2$  and  $^{13}\text{C}^{16}\text{O}_2$  isotopologs of  $\text{CO}_2$ . Agreement between concentration measurements and the virial-corrected ideal-gas law is shown to be within 0.5% for  $^{12}\text{C}^{16}\text{O}_2$  and 12% for  $^{13}\text{C}^{16}\text{O}_2$ , with the measured ratio in excellent agreement with that expected from the natural

abundance of both isotopes. The measurement technique is demonstrated to be highly linear, with deviation from a linear measurement being  $(-4.9 \pm 8.5)\%$  over a concentration range of 3 orders of magnitude. These results demonstrate the ability of DFCS to correctly measure the relative concentrations of isotopologs with high precision, accuracy, and a large dynamic range, making it a promising technique for measurements for environmental monitoring and biomedical sciences.

#### ACKNOWLEDGMENTS

This work was supported by Australian Research Council Linkage Project Grants (Grants No. LP120200605 and No. LP140100647) and the Government of South Australia (The Premiers Science and Research Fund).

- [1] R. J. Francey, C. E. Allison, D. M. Etheridge, C. M. Trudinger, I. G. Enting, M. Leunberger, R. L. Langenfelds, E. Michel, and L. P. Steele, A 1000-year high precision record of  $\delta^{13}\text{C}$  in atmospheric  $\text{CO}_2$ , *Tellus B* **51**, 170 (1999).
- [2] T. K. Bauska, D. Baggenstos, E. J. Brook, A. C. Mix, S. A. Marcott, V. V. Petrenko, H. Schaefer, J. P. Severinghaus, and J. E. Lee, Carbon isotopes characterize rapid changes in atmospheric carbon dioxide during the last deglaciation, *Proc. Natl. Acad. Sci.* **113**, 3465 (2016).
- [3] M. S. Torn, S. C. Biraud, C. J. Still, W. J. Riley, and J. A. Berry, Seasonal and interannual variability in  $^{13}\text{C}$  composition of ecosystem carbon fluxes in the U.S. Southern great plains, *Tellus B: Chem. Phys. Meteorol.* **63**, 181 (2011).
- [4] D. Yakir and L. da S. L. Sternberg, The use of stable isotopes to study ecosystem gas exchange, *Oecologia* **123**, 297 (2000).
- [5] W. G. Mook,  $^{13}\text{C}$  in atmospheric  $\text{CO}_2$ , *Netherlands J. Sea Res.* **20**, 211 (1986).
- [6] A. C. Mix, N. G. Pisias, R. Zahn, W. Rugh, C. Lopez, and K. Nelson, Carbon 13 in pacific deep and intermediate waters, 0–370 ka: Implications for ocean circulation and pleistocene  $\text{CO}_2$ , *Paleoceanography* **6**, 205 (1991).
- [7] S. S. Assonov, C. A. M. Brenninkmeijer, T. J. Schuck, and P. Taylor, Analysis of  $^{13}\text{C}$  and  $^{18}\text{O}$  isotope data of  $\text{CO}_2$  in CARIBIC aircraft samples as tracers of upper troposphere/lower stratosphere mixing and the global carbon cycle, *Atmos. Chem. Phys.* **10**, 8575 (2010).
- [8] B. Galfond, D. Riemer, and P. Swart, Analysis of signal-to-noise ratio of  $\delta^{13}\text{C}$ - $\text{CO}_2$  measurements at carbon capture, utilization and storage injection sites, *Int. J. Greenhouse Gas Control* **42**, 307 (2015).
- [9] S. Krevor, J. C. Perrin, A. Esposito, C. Rella, and S. Benson, Rapid detection and characterization of surface  $\text{CO}_2$  leakage through the real-time measurement of  $^{13}\text{C}$  signatures in  $\text{CO}_2$  flux from the ground, *Int. J. Greenhouse Gas Control* **4**, 811 (2010).
- [10] T. H. Yang, E. Heinzle, and C. Wittmann, Theoretical aspects of  $^{13}\text{C}$  metabolic flux analysis with sole quantification of carbon dioxide labeling, *Comput. Biol. Chem.* **29**, 121 (2005).

- [11] E. R. Crosson, K. N. Ricci, B. A. Richman, F. C. Chilesse, T. G. Owano, R. A. Provencal, M. W. Todd, J. Glasser, A. A. Kachanov, B. A. Paldus, T. G. Spence, and R. A. Zare, Stable isotope ratios using cavity ring-down spectroscopy: Determination of  $^{13}\text{C}/^{12}\text{C}$  for carbon dioxide in human breath, *Anal. Chem.* **74**, 2003 (2002).
- [12] D. Dickinson, S. Bodé, and P. Boeckx, Measuring  $^{13}\text{C}$ -enriched  $\text{CO}_2$  in air with a cavity ring-down spectroscopy gas analyser: Evaluation and calibration, *Rapid Commun. Mass Spectrom.* **31**, 1892 (2017).
- [13] R. N. Zare, D. S. Kuramoto, C. Haase, S. M. Tan, E. R. Crosson, and N. M. R. Saad, High-precision optical measurements of  $^{13}\text{C}/^{12}\text{C}$  isotope ratios in organic compounds at natural abundance, *Proc. Natl. Acad. Sci.* **106**, 10928 (2009).
- [14] J. Mohn, M. J. Zeeman, R. A. Werner, W. Eugster, and L. Emmenegger, Continuous field measurements of  $\delta^{13}\text{C}$  –  $\text{CO}_2$  and trace gases by FTIR spectroscopy, *Isotopes Environ. Health Stud.* **44**, 241 (2008).
- [15] D. W. T. Griffith, M. B. Esler, and S. R. Wilson, Isotopic analysis of atmospheric trace gases by FTIR spectroscopy, *AIP Conf. Proc.* **430**, 207 (1998).
- [16] G. B. Rieker, F. R. Giorgetta, W. C. Swann, J. Kofler, A. M. Zolot, L. C. Sinclair, E. Baumann, C. Cromer, G. Petron, C. Sweeney, P. P. Tans, I. Coddington, and N. R. Newbury, Frequency-comb-based remote sensing of greenhouse gases over kilometer air paths, *Optica* **1**, 290 (2014).
- [17] M. J. Thorpe, D. Balslev-Clausen, M. S. Kirchner, and J. Ye, Cavity-enhanced optical frequency comb spectroscopy: Application to human breath analysis, *Opt. Express* **16**, 2387 (2008).
- [18] F. Adler, M. J. Thorpe, K. C. Cossel, and J. Ye, Cavity-enhanced direct frequency comb spectroscopy: Technology and applications, *Annu. Rev. Anal. Chem.* **3**, 175 (2010).
- [19] D. R. Carlson, D. D. Hickstein, A. Lind, S. Droste, D. Westly, N. Nader, I. Coddington, N. R. Newbury, K. Srinivasan, S. A. Diddams, and S. B. Papp, Self-referenced frequency combs using high-efficiency silicon-nitride waveguides, *Opt. Lett.* **42**, 2314 (2017).
- [20] P. Del’Haye, A. Schliesser, O. Arcizet, T. Wilken, R. Holzwarth, and T. J. Kippenberg, Optical frequency comb generation from a monolithic microresonator, *Nature* **450**, 1214 (2007).
- [21] B. Stern, X. Ji, Y. Okawachi, A. L. Gaeta, and M. Lipson, Battery-operated integrated frequency comb generator, *Nature* **562**, 401 (2018).
- [22] L. C. Sinclair, J.-D. Deschênes, L. Sonderhouse, W. C. Swann, I. H. Khader, E. Baumann, N. R. Newbury, and I. Coddington, Invited article: A compact optically coherent fiber frequency comb, *Rev. Sci. Instrum.* **86**, 081301 (2015).
- [23] E. M. Waxman, K. C. Cossel, G.-W. Truong, F. R. Giorgetta, W. C. Swann, S. Coburn, R. J. Wright, G. B. Rieker, I. Coddington, and N. R. Newbury, Intercomparison of open-path trace gas measurements with two dual-frequency-comb spectrometers, *Atmos. Meas. Tech.* **10**, 3295 (2017).
- [24] N. Bourbeau Hébert, S. Scholten, R. White, J. Genest, A. Luiten, and J. Anstie, A quantitative mode-resolved frequency comb spectrometer, *Opt. Express* **23**, 13991 (2015).
- [25] S. K. Scholten, J. D. Anstie, N. Hébert, R. W. White, J. Genest, and A. N. Luiten, Complex direct comb spectroscopy with a virtually imaged phased array, *Opt. Lett.* **41**, 1277 (2016).
- [26] S. K. Scholten, C. Perrella, J. D. Anstie, R. T. White, W. Al-Ashwal, N. Bourbeau Hébert, J. Genest, and A. N. Luiten, Number-Density Measurements of  $\text{CO}_2$  in Real Time With an Optical Frequency Comb for High Accuracy and Precision, *Phys. Rev. Appl.* **9**, 054043 (2018).
- [27] M. Shirasaki, Large angular dispersion by a virtually imaged phased array and its application to a wavelength demultiplexer, *Opt. Lett.* **21**, 366 (1996).
- [28] S. A. Diddams, L. Hollberg, and V. Mebele, Molecular fingerprinting with the resolved modes of a femtosecond laser frequency comb, *Nature* **445**, 627 (2007).
- [29] L. S. Rothman *et al.*, The HITRAN 2012 molecular spectroscopic database, *J. Quant. Spectrosc. Radiat. Transfer* **130**, 4 (2013).
- [30] L. S. Rothman *et al.*, The HITRAN molecular spectroscopic database and HAWKS (HITRAN Atmospheric Workstation): 1996 edition, *J. Quant. Spectrosc. Radiat. Transfer* **60**, 665 (1998).
- [31] R. R. Gamache, R. L. Hawkins, and L. S. Rothman, Total internal partition sums in the temperature range 70–3000 K: Atmospheric linear molecules, *J. Mol. Spectrosc.* **142**, 205 (1990).
- [32] R. Kakkar, *Atomic and Molecular Spectroscopy: Basic Concepts and Applications* (Cambridge University Press, Delhi, India, 2015).
- [33] J. T. Hodges, J. Tennyson, P. F. Bernath, A. Campargue, A. Csaszar, L. Daumont, R. R. Gamache, D. Lisak, O. Naumenko, L. Rothman, H. Tran, N. Zobov, B. Chris, L. Gianfrani, and J. M. Hartmann, Recommended isolated-line profile for representing high-resolution spectroscopic transitions (IUPAC Technical Report), *Pure Appl. Chem.* **86**, 1931 (2014).
- [34] N. H. Ngo, N. Ibrahim, X. Landsheere, H. Tran, P. Chelin, M. Schwell, and J.-M. Hartmann, Intensities and shapes of  $\text{H}_2\text{O}$  lines in the near-infrared by tunable diode laser spectroscopy, *J. Quant. Spectrosc. Radiat. Transfer* **113**, 870 (2012).
- [35] V. P. Kochanov, On systematic errors in spectral line parameters retrieved with the Voigt line profile, *J. Quant. Spectrosc. Radiat. Transfer* **113**, 1635 (2012).
- [36] D. Lisak and J. T. Hodges, Low-uncertainty  $\text{H}_2\text{O}$  line intensities for the 930-nm region, *J. Mol. Spectrosc.* **249**, 6 (2008).
- [37] I. E. Gordon *et al.*, The HITRAN 2016 molecular spectroscopic database, *J. Quant. Spectrosc. Radiat. Transfer* **203**, 3 (2017).
- [38] P. De Bièvre, M. Gallet, N. E. Holden, and I. L. Barnes, Isotopic abundances and atomic weights of the elements, *J. Phys. Chem. Ref. Data* **13**, 809 (1984).
- [39] A. F. Estrada-Alexanders, O. Guzmán, and B. Pérez-Vidal, High-precision virial coefficients of argon and carbon dioxide from integration of speed of sound data in the pressure-temperature domain, *Mol. Phys.* **110**, 1349 (2012).
- [40] R. A. Johnson, *Miller & Freund’s Probability and Statistics for Engineers*, 7th ed. (Pearson Prentice Hall, Upper Saddle River, N.J., 2005).
- [41] Statistics LET Subcommands: Weighted Standard Deviation, Tech. Rep. (National Institute of Standards and Technology (NIST), 1996).